Landslides (2019) 16:1731–1744
DOI 10.1007/s10346-019-01241-4
Received: 19 February 2019
Accepted: 4 July 2019
Published online: 17 July 2019

Zhen-lei Wei · Yue-quan Shang · Hong-yue Sun · Hao-di Xu · Dong-fei Wang

The effectiveness of a drainage tunnel in increasing the rainfall threshold of a deep-seated landslide

Abstract A rising level of groundwater is a critical trigger for deep-seated landslides. Accordingly, an effective measure to improve the stability of a landslide is to reduce the groundwater level of a slope by using a drainage system. This study investigates the effectiveness of drainage tunnels in increasing the rainfall threshold of a deep-seated landslide. Monitoring results show that the movement of the landslide is highly sensitive to the prevailing groundwater level (GL), and the value of GL has a direct connection with the movement of a slope. Based on continuous monitoring of data of groundwater level (GL) and precipitation, the Particle Swarm Optimization Support Vector Machine (PSO-SVM) model was developed to predict GL based on antecedent rainfall. The calculated results show that the performance of the PSO-SVM model is acceptable. Using intensity-duration-frequency (IDF) analysis and the PSO-SVM model, the rainfall threshold of the landslide in this study was estimated to range from 63 to 78 mm before the drainage tunnel was completed. This contrasted with a rainfall threshold ranging from 144 to 162 mm after the drainage tunnel was completed. This shows that the construction of a drainage tunnel increased the rainfall threshold of the landslide significantly, nearly doubling it.

Keywords Groundwater · Rainfall threshold · Drainage tunnel

Introduction

Landslide disasters often occur during rainy seasons. Rainfall-induced landslides are generally caused by changes in the pore water pressures which lead to a reduction of soil strength and consequently slope instability. These changes are often caused by an increase in the saturation degree of the soils (initially unsaturated) above the infiltration front (Iverson 2000; Godt et al. 2009; Zhang et al. 2015), by the formation of a perched water table in the top soil layers (Shackelford et al. 1994) or by an increase in the groundwater level (Corominas et al. 2005; Ledesma et al. 2009; Conte et al. 2018). In the former two cases, the landslide is generally shallow and a relatively small volume of soil is involved. By contrast, in the latter case, the landslide is generally very deep and involves a great volume of soil. This is the case considered in the present study. In the case of a deep-seated landslide, the rise of the groundwater level often induces a landslide. Mantovani et al. (2000) monitored the Tessina landslide in northeastern Italy and concluded that the landslide was associated with an increase in the groundwater level during the observation period. Zhi et al. (2016) investigated and monitored a rainfall-induced, deep-seated landslide in Zhejiang Province, China, and concluded that the groundwater level had a direct connection with the movement of the slope. Therefore, it is very important to evaluate the fluctuation of the groundwater level accurately based on antecedent rainfall in order to predict the occurrence of a deep-seated landslide.

As an increase in groundwater level is a critical trigger for a deep-seated landslide, improving the stability of the landslide by reducing the groundwater level of the slope through drainage works during rainy seasons is effective. Current drainage works can be divided into two main categories: surface water drainage works and subsurface drainage works (Wang et al. 2013). The main objective of surface water drainage systems is to protect the surface runoff infiltrating into the slope to increase the groundwater level. Conte and Troncone (2018) proposed a method to the design of drainage trenches used to control the mobility of translational landslides periodically activated by rainfall. Cotecchia et al. (2016) verified the effects of drainage trenches through a combination of finite element modeling of seepage and limit equilibrium analyses. However, intercepting gutters and drainage trenches often cannot effectively prevent rainfall infiltration due to their poor performance in trapping water (Sun et al. 2010). Subsurface drainage works are divided mainly into drainage holes and drainage tunnels. Rahardjo et al. (2003) examined the effectiveness of drainage holes in stabilizing residual soil slopes against rainfall-induced slope failures in a tropical climate. Field monitoring results indicate that using drainage holes to lower the water table can have beneficial results. However, drainage holes are always blocked due to different constraints associated with construction technology, which makes their long-term reliability questionable (Sun et al. 2010). On the other hand, underground drainage tunnels are ideal for intercepting or guiding underground water in deep water-bearing strata and can improve the effectiveness and reliability of drainage. Sun et al. (2010) discussed the effectiveness of a drainage tunnel together with anti-slide piles on a deep-seated landslide control based on real-time and synchronic monitoring. The results of their study showed that an underground drainage tunnel can effectively lower the level of rising underground water induced by rainfall. Wang et al. (2013) proposed a method to determine the optimal location of drainage tunnels based on numerical simulations. Matti et al. (2012) evaluated the impact of a deep drainage tunnel with sub-vertical drainage boreholes towards the surface on reducing deformation velocities and increasing a landslide's safety factor in Vaud, Switzerland.

Despite the benefits of drainage tunnels, it is still uncommon for the engineering community to use drainage tunnels as a major engineering measure to control landslides. The main reason is that their drainage effect has not yet been fully validated by engineering practice (Sun et al. 2010), and the engineering community is still doubtful about the effectiveness of drainage tunnels. Therefore, at present, drainage tunnels are generally regarded only as a supplementary measure for landslide control. In addition, the effectiveness of current drainage works is usually described in terms of an increase in the slope factor of safety compared to the factor of safety for cases without drainage works. The factor of safety (FS) is usually calculated by numerical models. Uncertainties about the soil's shear strength parameters make the calculation of FS uncertain, and this in turn makes the approach rather weak. It would be

more convincing to evaluate the effectiveness of drainage works based on field monitoring.

In this study, based on monitoring data relating to rainfall, groundwater level, and surface displacement, we discuss the effectiveness of drainage tunnels in increasing the rainfall threshold of a deep-seated landslide. The monitoring results show that deep-seated landslides are highly sensitive to groundwater level (GL). The stability of the slope is determined by the value of GL directly. So, if we could predict the value of GL based on antecedent rainfall accurately, we could obtain the rainfall threshold of deep-seated landslides. The particle swarm optimization support vector machine (PSO-SVM) method is used to predict the value of GL under different rainfall conditions. Based on the PSO-SVM model, the value of GL before and after the completion of drainage tunnels induced by identical rainfall is also compared. Through intensity-duration-frequency (IDF) curves, we also examine the effectiveness of drainage tunnels on an increasing rainfall threshold of the landslide.

Study area and data collection

The study area is located in Changshan County, Zhejiang Province, China, where the average annual precipitation is about 1800 mm. Rainfall is concentrated mostly from May to July. The landslide under study is a remobilized ancient landslide deposit formed by highway construction (Sun et al. 2018). The main slip direction of the landslide is in a northerly direction. The landslide is approximately 350 m long from south to north and 140 m wide at the front edge and 55 m wide at the trailing edge. The boundary of the landslide is controlled by cracks 1, 3, and 4 (Fig. 1). The trailing edge of the landslide is located at an elevation of 620 m in the southern part of the site where a tensile crack 4 is developing. The leading edge is located at an elevation of 510 m in the northern part of the site. The landslide has an average slope of 20° (Fig. 1).

The formation lithology in the slope area is composed mainly of Quaternary Residual Soil Formation (Q), conglomerate and mudstone of the Upper Jurassic Huangjian Formation (J3h), mudstone, and carbonaceous mudstone of the Lower Ordovician Ningguo Formation (O1n) (Fig. 2). The location of the slip surface was determined by the three deep inclinometers, JC-1, JC-2, and JC-3. The locations of the three deep inclinometers are shown in Fig. 1. The deepest deformation of JC-1 was located at a depth of approximately 18.7 m, whereas those of JC-2 and JC-3 were located at depths of approximately 20.3 m and 22.5 m. According to the distributions of formations at the drilling holes, the depths of the surface between the J3h and On1 at JC1, JC2, and JC3 are 18.1 m, 17.8 m, and 22.5 m, respectively (Sun et al. 2018). The deepest deformations of inclinometers are found near the location of the unconformity surface. Through the above analysis, the landslide body is mainly overlying Jurassic strata, and the slip surface is along the unconformity surface between the J3h and On1 strata. The location of the slip surface is indicated in Fig. 2. After careful surveying, it is concluded that the groundwater is mainly distributed in the Quaternary residual soil and Jurassic strata in the loss cover, and the aquifer thickness is approximately 17–38 m (Sun et al. 2018). The locations of the initial groundwater level were decided by drilling holes (D1, D2, D3, and D4).

During construction of a highway, several cracks formed on the surface of the slope. Figure 1 shows four major cracks in the study area. Crack 1, which is 177 m long and 5 to 10 cm wide, is located on the western boundary of the landslide. Crack 2 is located on the middle part of the landslide and has a maximum width of 8 cm. Crack 3 is located on the eastern boundary of the landslide. The maximum width of the crack is approximately 15 cm. Crack 4 is located in the upper part of the landslide and extends in two directions. One part extends in a northwesterly direction; the other extends in a northerly direction and intersects with crack 3. The cracks occurred at different times as a result of a winding mountain road that crosses the slope and has been subject to multiple excavations. The overall deformation of the slope will be like a partial deformation due to the segmentation of the road. However, in this case, the landslide is considered a deep-seated landslide based on GPS monitoring data and deep inclinometer data. Detailed information on the deformation mechanisms of the deep-seated landslide can be found in Sun et al. (2018).

To ensure the safety of the construction, data relating to the groundwater level, the surface deformation, and rainfall in the landslide were monitored from January 2016. An automatic water-level recorder was installed at the bottom of the boreholes. The depth of the groundwater was evaluated from the bottom of each borehole, and the groundwater level was monitored hourly using pressure-type water gauges within 2-mm accuracy. The rainfall data were collected by an automatic tipping bucket rain gauge that recorded rainfall every hour within 0.5-mm accuracy. Surface deformation was monitored by GPS devices within an accuracy of 2 mm. The position of the monitoring instrument is shown in Fig. 1.

There are four piezometers and six GPS locations. An analysis of monitoring data from three GPS stations (M3, M4, M5) showed similar patterns of landslide movements across the central part of the landslide area, but at different velocities. Large displacement was recorded in the central part of the landslide (M3, M4, M5), and small displacements were identified along the landslide boundaries (M1, M6, M2). The position inside the landslide area with maximal displacement in the monitoring period was the main criterion for selecting M5 as the most representative for the analyses of the movement of the Qili landslide. Data that monitored groundwater levels at the four locations within the landslide showed similar patterns of changes in the groundwater levels. Data records from water level sensor W3, which was installed at the central monitoring station, show the strongest relation to the M5 data. Data measured with other water level sensors generally show smaller relative change between maximal and minimal groundwater levels. Therefore, the W3 sensor data were most representative of the behavior of the Qili landslide and, in combination with the M5 data, were used for landslide prediction.

After a detailed investigation, a drainage tunnel was also built below the landslide to prevent the rapidly increasing GL (Fig. 3). The construction of the drainage tunnel began in August 2016 and was completed in November 2016. It was constructed in the intact bedrock below the slip surface of the landslide. Its span and height were 2 m and 2.25 m, respectively. The length of the drainage tunnel was about 305 m. It was used to intercept the rainfall and lower the groundwater level in the landslide.

Correlation between the groundwater level and surface displacement

A high groundwater level (GL) always corresponds with a rapid landslide movement. The relationship between groundwater level and cumulative surface displacement is shown in Fig. 4. The

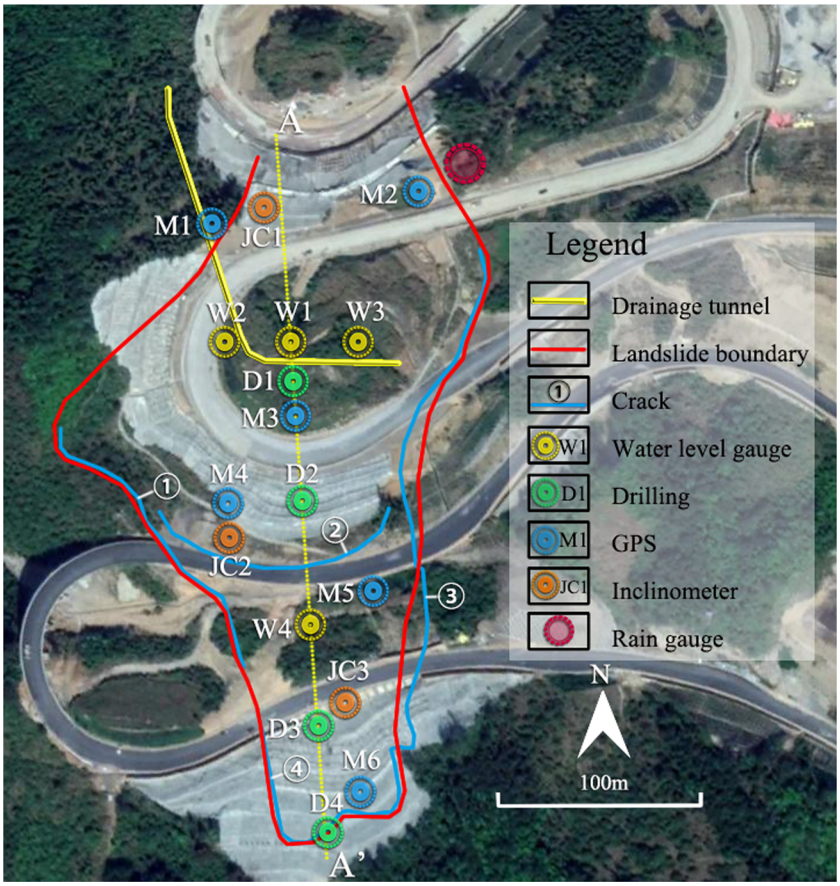

Fig. 1 Engineering geologic plane with monitoring points

direction of surface displacement is north. The total measured surface displacement is 80 mm. The average annual velocity of the landslide during the monitoring period was 40 mm/year. Figure 4 shows two periods of faster movements. The maximal velocity observed was 3 mm/day and occurred in the second period of faster movement during the last week of June 2017. The longest period of faster movement lasted from the end of April 2016 to the end of July 2016, during which the total displacement was 40 mm. Both periods of faster movement occurred as a consequence of rising groundwater levels (Fig. 4).

In order to explore the relationship between GL and surface displacement during fast movement periods, recording GL and

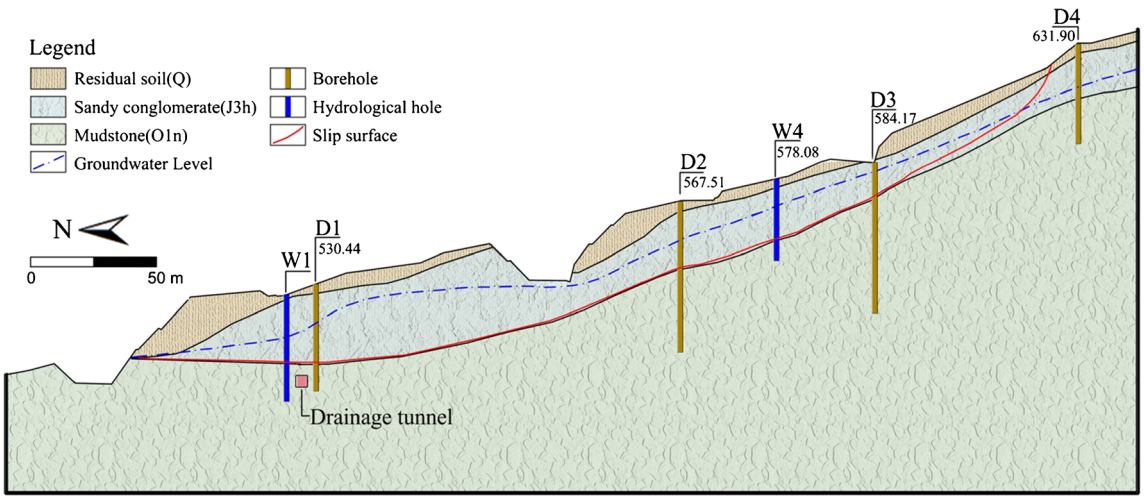

Fig. 2 The engineering geologic cross-section of A-A'

Fig. 3 Outlet of the drainage tunnel

surface displacement during these periods is presented in detail in Figs. 5 and 6. The relationship between GL and surface displacement before the drainage tunnel was completed is shown in Fig. 5a. Six obvious groundwater level peaks (PGL), PGL1–PGL6, can be observed in Fig. 5a. It can also be seen that the variation of displacement and GL did not change synchronously. When the value of GL is smaller than a critical value (e.g., the segment between February and early April), the displacement curve is quite flat, with negligible fluctuations. When the GL is higher than a critical level (e.g., the six groundwater level peaks PGL1–PGL6), the displace curve increases dramatically, which indicates that rapid landslide movement occurred. The displacement velocity is also calculated and plotted with the groundwater level in Fig. 5b. Six distinct displacement velocity peaks (PDV), PDV1–PDV6, on the velocity curve can also be observed. This study's observations show a one-to-one correspondence between PGL and PDV. When the GL reaches peak point, displacement velocity also reaches peak point.

We also explore the relationship between the groundwater level (GL) and cumulative surface displacement after the drainage tunnel was completed, as shown in Fig. 6. It can also be seen that the variation of displacement and GL could not change synchronously. When GL is higher than the critical GL (31 m), the displacement curve will also increase rapidly. We also found that there is one-to-one correspondence between PGL and PDV. When the GL reaches peak point, the displacement velocity also reaches peak point.

The details of PDVs and PGLs are listed in Table 1, which shows that the movement of a deep-seated landslide is highly sensitive to GL, and that the value of GL determines the motion state of the landslide directly. In this study, the critical groundwater level that induces rapid movement is approximately 31 m.

Because of the importance of groundwater level in assessing the stability of a landslide, monitoring GL could serve as an early warning of a landslide. Once the GL is close to, or larger than, the critical value (31 m in this study), the landslide will have the possibility of moving. If the value of GL could be predicted based on the antecedent rainfall, then by comparing the predicted GL with critical GL, the motion state of the landslide could be estimated; in other words, the rainfall threshold of the landslide would be obtained.

Correlation between groundwater level and rainfall

Figure 7 presents observations of GL response to rainfall over approximately 2 years. In order to further explore the relationship between critical rainfall and GL, this study explores the data of the monitoring period during which GL reached a critical level (31 m) in more detail in Fig. 7b, c. Before the construction of the drainage tunnel, the total rainfall amount was about 1196 mm (01/04/2016–01/08/2016) (Fig. 7b) and the maximum daily rainfall was about 79.5 mm (05/06/2016). The highest groundwater level during this

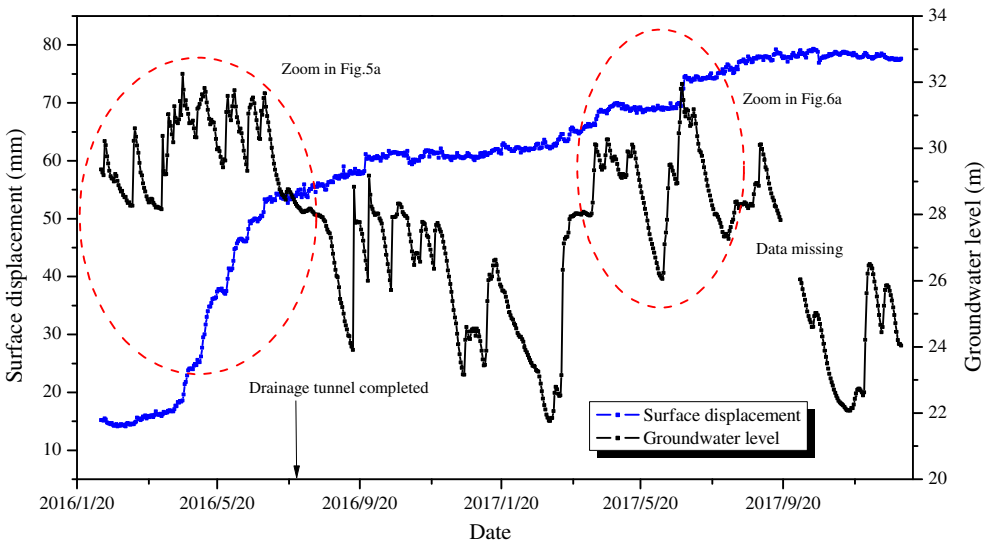

Fig. 4 Relationship between the groundwater level (GL) and cumulative surface displacement

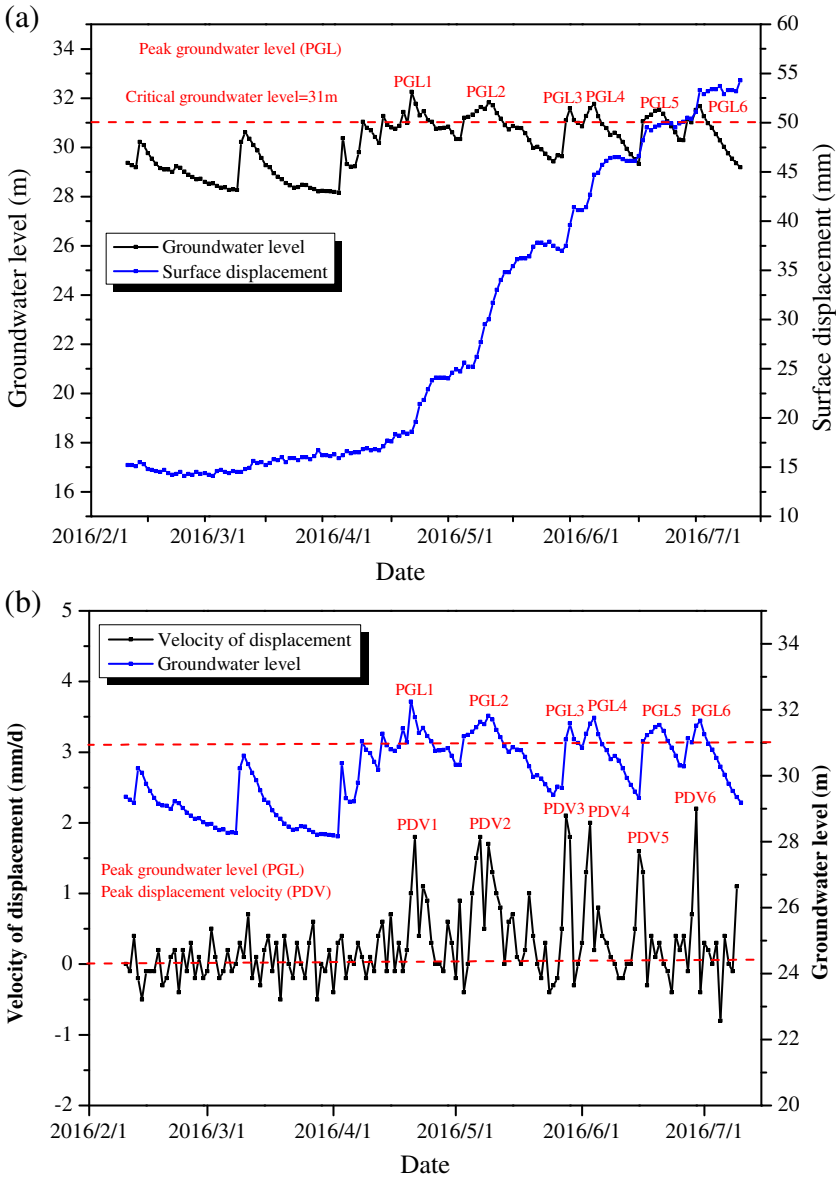

Fig. 5 Relationship between displacement and groundwater level before the drainage tunnel was completed: **a** relationship between cumulative displacements and groundwater level. **b** Relationship between displacement velocity and groundwater level

period was about 32 m. Before the drainage tunnel was completed, the GL easily reached critical value (31 m). In fact, GL reached critical value six times. Total rainfall after the construction of the drainage tunnel during the same season was about 1209 mm (01/04/2017–01/08/2017) (Fig. 7c). The maximum daily rainfall was about 140.5 mm (24/06/2017). After completion of the drainage tunnel, the GL decreased rapidly and remained at a relatively low level. There was only one time when the GL reached critical value. Comparing the total amount of rainfall, the amount of rain after construction of the drainage tunnel was greater than the total rainfall amount before the construction of the tunnel. However, GL reached critical value only once. Furthermore, the lowest groundwater level also decreased after completion of the drainage tunnel. Before completion of the tunnel, the lowest groundwater level was about 28 m after a long dry period. After the drainage tunnel was completed, the lowest groundwater level was about 26 m after a long dry period. The lower groundwater level means the more difficult it became for the GL to increase during the next rainfall. Figure 7a shows that the drainage tunnel successfully controlled the increase in the groundwater level. As the value of GL directly determines the motion state of the landslide, it means the displacement reduction recorded after the tunnel was installed can be ascribed to the presence of the drainage tunnel.

The close relationship between rainfall and groundwater level is a necessary requirement for the proposed approach. The premise of landslide prediction in this study is that landslide movement depends on GL depth and that GL depth depends on precipitation. It is first necessary to predict GL depth from the precipitation data and then compare the predicted GL depth with critical GL to verify the stability of the slope. If the predicted GL is larger than the

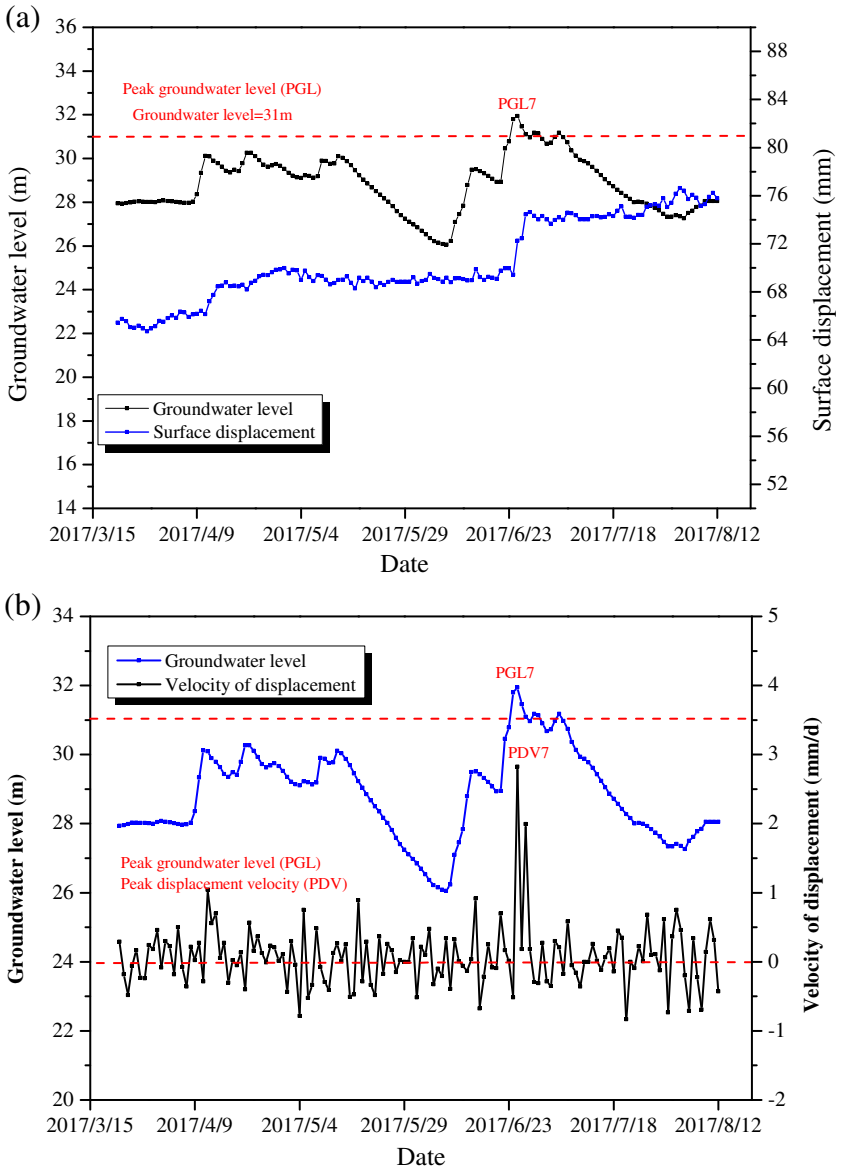

Fig. 6 Relationship between the groundwater level (GL) and cumulative surface displacement after the drainage tunnel was completed. **a** Relationship between cumulative displacements and groundwater level. **b** Relationship between displacement velocity and groundwater level

critical GL, the slope will probably demonstrate an instability trend. If the predicted GL is smaller than the critical GL, the slope will be considered safe. When using methods to construct a model for predicting GL, determining the output variable is important because it may influence the accuracy of the forecasts. Currently, two different output variables are used, i.e., (1) the elevation of groundwater level (GL) and (2) the groundwater level fluctuation (GLF), which is defined as the difference between the current and subsequent GL data. Hong (2017) evaluated that the effects two different output variables had on the accuracy of the forecasts and found that the forecasting method that used GLF had much better agreement with the measured values than GL. Also, Krkač et al. (2017) concluded that predictions of changes in GLF yielded significantly better results than direct predictions of GL. In this study, the GLF approach is used. Groundwater level fluctuation (GLF)

Table 1 Statistical data of PGL and PDV

Number	Monitor date	PGL (m)	PDV (mm/day)
1	April 21/2016	31.8	1.8
2	May 7/2016	31.6	1.8
3	May 28/2016	31.1	2.1
4	June 3/2016	31.6	2.0
5	June 15/2016	31.1	1.6
6	June 29/2016	31.5	2.2
7	June 25/2017	31.9	2.8

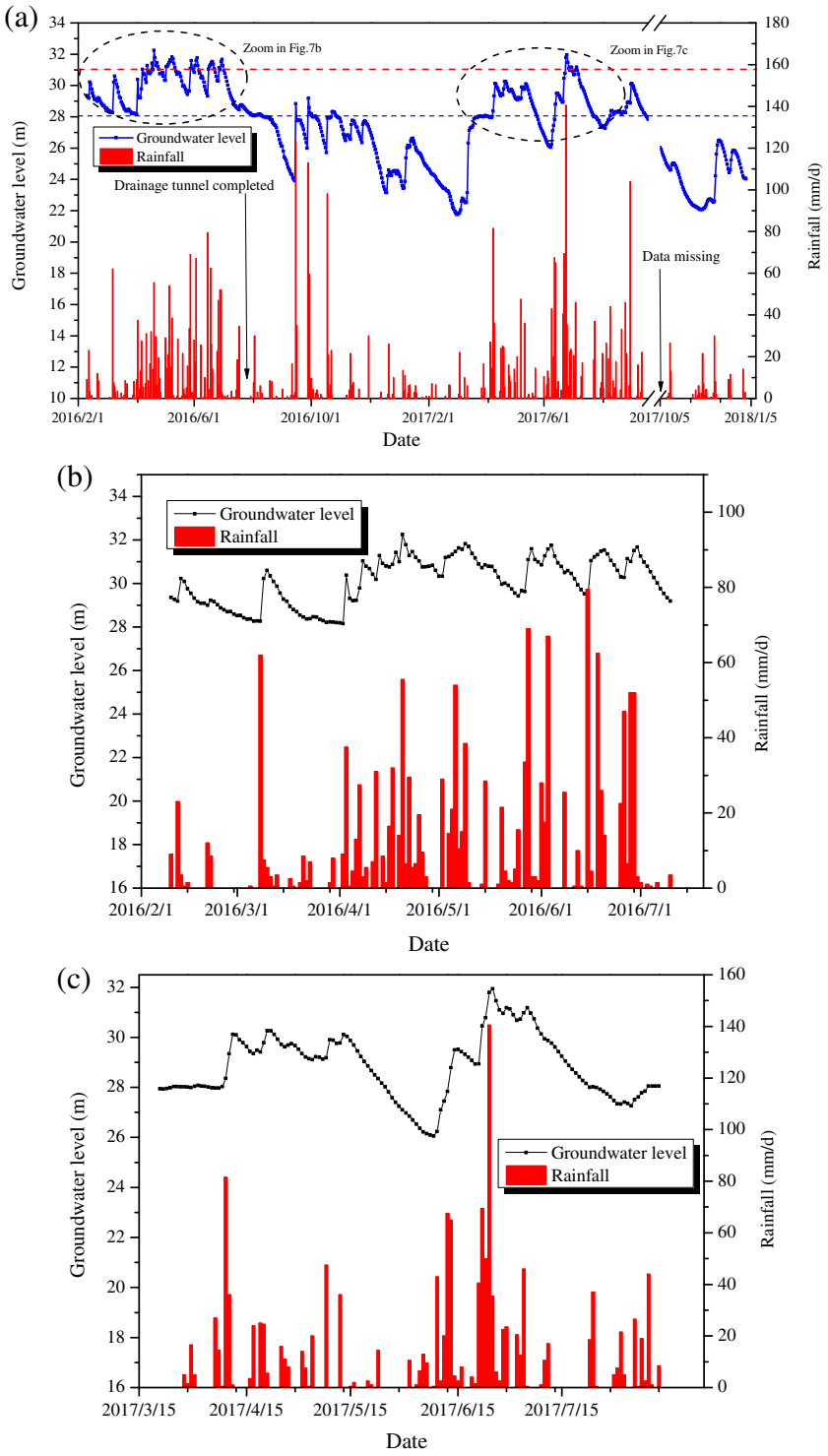

Fig. 7 Relationship between rainfall and GL. **a** Total monitoring period, **b** before the drainage tunnel was completed, and **c** after the drainage tunnel was completed

manifests in two ways: (1) increased by rainfall named as GLFR and (2) decreased by drainage named as GLFD, where the latter refers to the speed at which the groundwater level descends. The relationships of GLF, GLFR, and GLFD are shown in Eq. (1).

$$\mathrm{GLF} = \mathrm{GLFR} + \mathrm{GLFD} \tag{1}$$

The GLFD is usually affected by the groundwater level and hydrogeological conditions of the slope. High groundwater levels are usually associated with large GLFD in order to maintain the groundwater balance in the body of the slope. The value of GLFD is usually the descending speed of GL under no precipitation. As the monitoring period during which the GL reaches critical level

(31 m) is more important for the stability of the slope, only monitoring data recorded when the GL settles at a high level are used. In this study, monitoring data from February 8, 2016 to July 2, 2016 (before the drainage tunnel was completed) and data from March 28, 2017 to July 14, 2017 (after the drainage tunnel was completed) are used. To determine the value of GLFD, the values of GLF and the corresponding GL are presented as shown in Fig. 8. It is considered that the lower enveloping curve (f(x)) represents the values of GLFD for different values of GL when there is no precipitation. The lower enveloping curves, (f(x)), before and after the drainage tunnel was completed are expressed as Eqs. (2) and (3), respectively. Equations (2) and (3) are concluded by automatic fitting. Equations (2) and (3) also have the minimum standard error.

$$y_{16} = 869.04 - 86.84 \times x_1 + 2.89 \times x_1^2 - 0.032 \times x_1^3 \quad (2)$$

$$y_{17} = 219.86 - 22.98 \times x_2 + 0.81 \times x_2^2 - 0.0093 \times x_2^3 \quad (3)$$

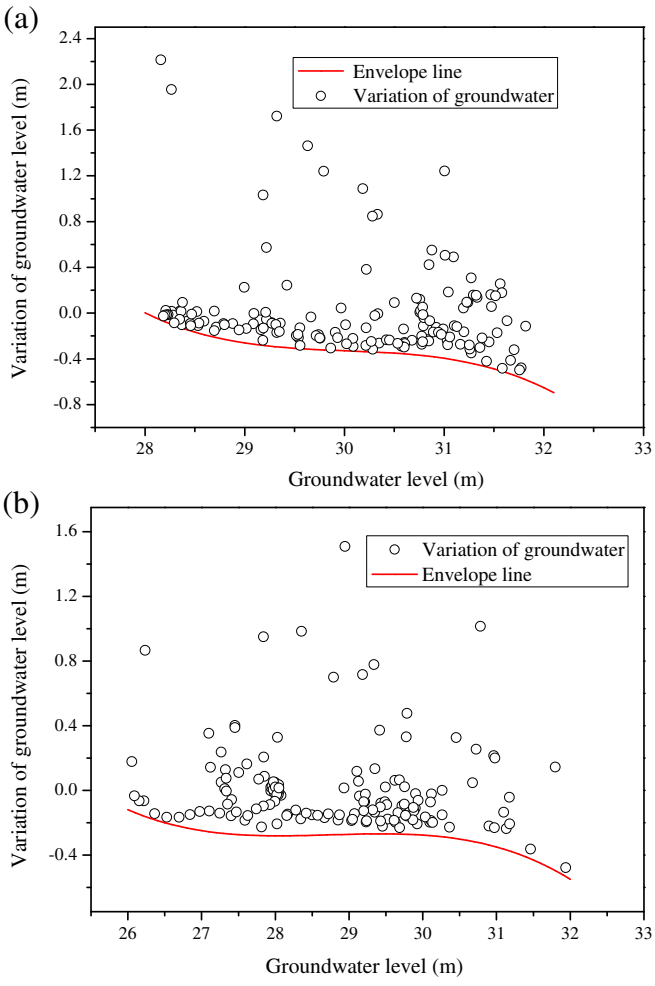

Fig. 8 Values of GLF and the corresponding GL: **a** before the drainage tunnel was completed and **b** after the drainage tunnel was completed

where y_{16} and y_{17} are the values of GLFD before and after the drainage tunnel was completed, for different GL values, and x_1 and x_2 are the corresponding groundwater levels before and after the drainage tunnel was completed, respectively. It should be noted that the proposed method has some limitations; the method is an empirically based method, and Eqs. (2) and (3) are only suitable for studying the landslide case.

Prediction of GLFR based on antecedent rainfall

PSO-SVM model

The support vector machine (SVM) is a kind of non-linear regression forecasting method that was proposed by Cortes and Vapnik (1995). The input variables are mapped into a higher-dimensional feature space through a non-linear transformation, a process that is used extensively in geotechnical engineering (Ji et al. 2016). In order to build an effective SVM model, the parameters of the model (C_s and γ) must be chosen properly in advance (Li and Kong 2014). The C_s is named as penalty parameter and the γ is named as kernel parameter. The parameter, C_s, determines the tradeoff cost between minimizing the training error and the complexity of the SVM model. With a larger C_s value, the predictive accuracy of the training sample is better. However, this may cause an over-training problem. The parameter, γ, of the kernel function defines a nonlinear mapping from the input space to the high-dimensional feature space. Hence, the parameters C_s and γ influence the efficiency and generalization performance of the SVM model (Zhou et al. 2016).

The Particle Swarm optimization (PSO) is an evolutionary algorithm developed in recent years (Bergh and Engelbrecht 2006). It is usually used for solving optimization problem. Each particle in the algorithm indicates a potential solution to the problem. The common feature is represented by position, speed, and fitness value. The fitness value can be calculated through the fitness function, which can estimate the merit of the particles. The velocity of the particle determines the movement direction and distance and adjusts dynamically with the movement experience of all the particles, so as to optimize the individual in the search-space (Ren et al. 2015). Considering the sensitivity of SVM to the model parameters, in this study, we used PSO to search for the optimal parameters, i.e., C_s and γ, of the SVM model for prediction.

In this section, based on the calculation of GLFR, the non-linear model, the PSO-SVM model, is considered for forecasting variations in the GLFR based on the antecedent rainfall. In order to verify the accuracy of the model's predictions, we used the root mean square error (RMSE) and relation index (RI), as defined below:

$$RMSE = \sqrt{\frac{1}{N}\sum_{i=1}^{N}(y_i - x_i)^2} \quad (4)$$

$$RI = \sqrt{1 - \frac{\sum_{i=1}^{N}(y_i - x_i)^2}{\sum_{i=1}^{N}\left(x_i - \overline{x_i}\right)^2}} \quad (5)$$

where x_i is the measured value, y_i is the predicted value, $\overline{x_i}$ is the average value of the sequence, and N is the number of predicted values.

Table 2 The Pearson correlation coefficient of different precipitation times

Pearson correlation coefficient	Before drainage tunnel completed	After drainage tunnel completed
S_1	0.62	0.78
S_2	0.51	0.71
S_3	0.44	0.60
S_4	0.39	0.51

The predicted value of GLFR in the future is usually considered to be a function of the precipitation that has occurred during the previous several days and the current precipitation. The influence of the period of antecedent precipitation, which has been widely debated in the literature, depends mainly on the hydrological conductivity of the landslide body. Effective antecedent precipitations are different in different cases. Some field monitoring data has shown that the time lag for peak precipitation and peak GL may be between 0.5 and 20 days (Lee et al. 2006). Park and Parker (2008) used 1-day precipitation to estimate infiltration for the next day. Hong and Wan (2011) chose 40-h precipitation as the influence duration of the previous rainfall. In this study, the Pearson correlation method is used to determine the duration of the influence (Dai and Lee 2001). It is considered that the variables in the correlation analysis to be the GLFR, the sum of precipitation on the same day and the previous day (S1), the sum of precipitation on the same day and the two previous days (S2), the sum of precipitation on the same day, and the previous 3 days (S3), the sum of precipitation on the same day and the previous 4 days (S4). Table 2 shows the Pearson correlation coefficient between GLFR and the different precipitation times.

Table 2 shows that S_1 had the best correlation with GLFR. The correlation coefficients will decrease with the passage of time, which means that the effect of precipitation will diminish in time. As the correlation coefficient of S_4 is quite small, 72 h (3 days) is selected as the influencing period. The initiation value of GL also has an effect on predicting results. Considering the results of the correlation analysis, the input parameters are defined as precipitation on the same day (P0), precipitation 1 day earlier (P1), precipitation 2 days earlier (P2), precipitation 3 days earlier (P3), and initiation GL (Krkač et al. 2017). The GLFR of future time is regarded as the output parameter. The precipitation from February 8, 2016 to June 7, 2016 and the precipitation from March 28, 2017 to June 20, 2017 (approximately 78% of the database) are selected as the training samples, and precipitation from June 12 to July 2, 2016 and precipitation from June 21 to July 14, 2017 (approximately 22% of the database) are selected as the test samples to verify the reliability of the model. A comparison between the forecasted results and the actual results before and after the drainage tunnel was completed is shown in Fig. 9.

Figure 9 shows that in 2016, before the drainage tunnel was completed, the RMSE and RI of the PSO-SVM model were 0.1 m and 0.97, respectively. In 2017, after the drainage tunnel was completed, the RMSE and RI of the PSO-SVM model were 0.09 m and 0.96, respectively. The results presented above show that the performance of PSO-SVM is acceptable. Therefore, the PSO-SVM model can represent the relationship between the influencing factors and GLFR and produce a good prediction of the GLFR.

To evaluate the effects of the drainage tunnel on decreasing GL further, the data of February 8, 2016 to June 7, 2016 are still regarded as training samples; however, rainfall from June 21 to July 14, 2017 is regarded as the input parameter of the test samples. The series values of predicted GLFR could be obtained and represent the variation of GLFR induced by rainfall events in 2017 under the condition of the uncompleted drainage tunnel. Then, the predicted GLFR and actual GLFR were compared. The actual GLFR represents the variation of GLFR induced by rainfall events in 2017 under the condition of the completed drainage tunnel. The rainfall condition that induces the predicted GLFR and actual GLFR is the same. The results of the comparison are shown in Fig. 10.

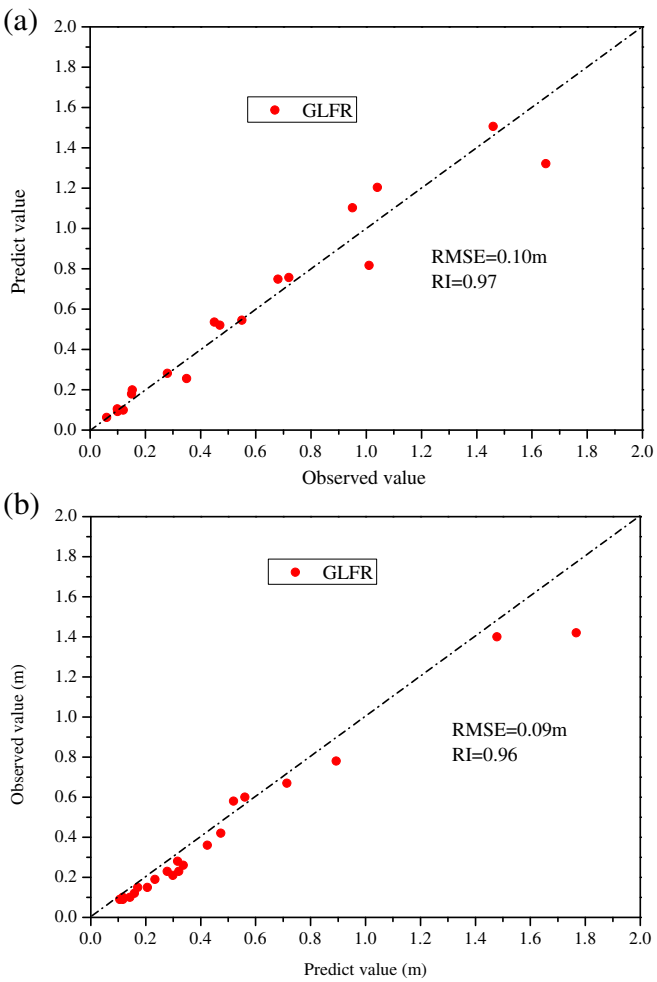

Fig. 9 Comparison of the forecast results and actual results **a** before the drainage tunnel and **b** after the drainage tunnel

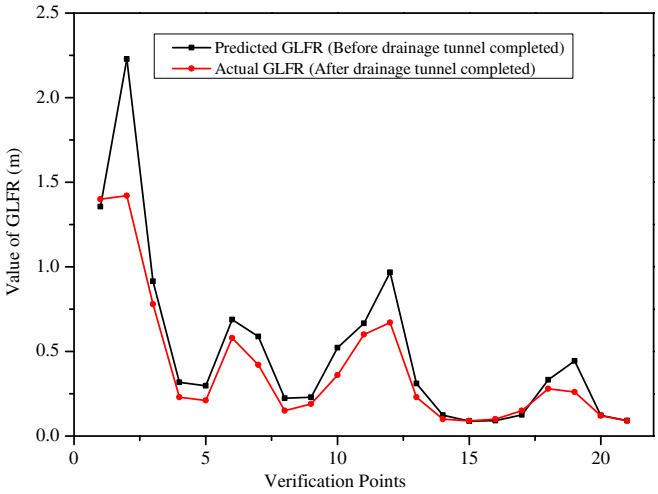

Fig. 10 Comparison of GLFR under the same rainfall conditions

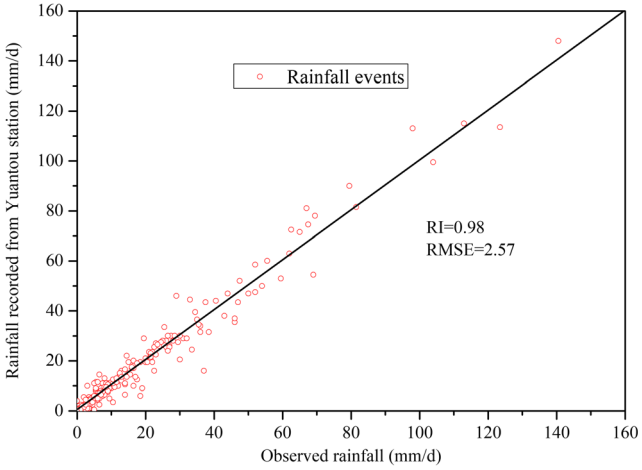

Fig. 11 Comparison between rainfall recorded from Yuantou station and observed rainfall

Figure 10 shows that the actual GLFR (after completion of the drainage tunnel) is much smaller than the predicted GLFR (before completion of the drainage tunnel) under the same rainfall condition. The peak value of predicted GLFR is about 2.2 m, in contrast with the peak value of actual GLFR, which is 1.4 m. This means that the drainage tunnel has reduced the increase of GL significantly under the same rainfall conditions.

Determine the rainfall threshold through IDF curves

IDF (intensity-duration-frequency) curves are routinely used in storm water and flood management design and predictions, as they describe the relationship linking duration and mean intensity of precipitation events characterized by the same return period (Bogaard and Greco 2018). The IDF curves are isolines of cumulative probability of precipitation events.

Several functional expressions can be used to describe such a relationship, most of which can be approximated, especially for durations longer than 1 h, as a power law:

$$I = A \times D^{B} \tag{6}$$

where I is the rainfall intensity (mm/h), D is the duration (h), B is the slope of the log-plotted straight line, and A is the measure of rain intensity of a rain event of unit duration (Bogaard and Greco 2018).

The IDF curves are determined based on the Atlas of Storms Statistical Parameters for Zhejiang Province (Zhejiang Province Bureau of Hydrology 2003). The distributions of the IDF curves are determined based on statistical results over many years from several meteorological stations. For different regions, the distribution of the IDF curves is also different. Note that the IDF curves are determined, for the most part, for rain durations of up to 24 h (Bogaard and Greco 2018). So, in this study, the durations of the IDF curves are selected as 1, 3, 6, and 24 h. Then, based on the Atlas, we were able to choose the specific IDF curves of the landslide site. In addition, to verify that the IDF curves used reflect the actual rainfall characteristics of the landslide site, the IDF curve was compared with the rainfall recorded from the nearest meteorological station, Yuantou station, which is about 1.2 km away from the landslide site. To verify that the spatial variability of rainfall characteristics between Yuantou station and the landslide site is small, the rainfall-monitoring recording (2016–2017) from Yuantou station was compared with the monitoring recording of the landslide site. The comparison is shown in Fig. 11.

The spatial variability of rainfall characteristics between Yuantou station and the landslide site is small. The RI and RMSE are 0.98 and 2.57, respectively, which means that the monitoring recording from Yuantou station reflected the actual rainfall characteristics of the landslide site. As rainfall has been monitored for a longer time at the Yuantou station, the IDF curves are compared with the rainfall recording from Yuantou station. The comparison is shown in Fig. 12. The 5-year return period means the maximum possible precipitation over a 5-year period. The 3-year return period means the maximum possible precipitation over a 3-year

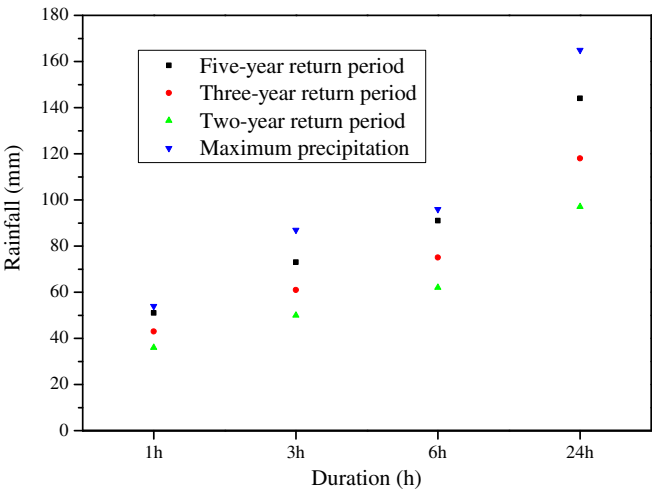

Fig. 12 Comparison of maximum precipitation with precipitation of a different return period

Table 3 Value of peak GL for different return period storms when the duration of the rainfall is 24 h

Return period (year)	Peak GL before drainage tunnel completed	Peak GL after drainage tunnel completed	Cumulative rainfall (mm)
2	31.41	30.16	96
3	31.81	30.65	120
5	32.37	30.97	144
10	32.72	31.26	178
20	33.09	31.50	216
50	33.36	31.65	252
100	33.66	31.72	312

period. The duration of recording rainfall from Yuantou station is approximately 5 years. So, if the maximum precipitation during recording is close to the precipitation of the 5-year return period, it means that the chosen IDF curves could reflect the actual rainfall characteristics at the landslide site. Figure 12 shows that the maximum precipitation recorded is slightly larger than the 5-year return period. The actual maximum precipitation recorded at Yuantou station is close to the precipitation of the 5-year return period from the IDF curves. This means that the chosen IDF curves could reflect the actual rainfall characteristics of the landslide site.

As the IDF curves of the landslide site were obtained, the depth of the precipitation of different return periods and durations were also obtained. Once the initial GLs were obtained, the proposed PSO-SVM model could be used to predict variations of GLFR. Figure 7a shows that the initial value of GL during the six groundwater level peaks (PGL1-PGL6) was about 29 m, so 29 m is regarded as the initial value of GL.

In order to consider the effect of antecedent rainfall on GL, a precipitation process is used as the input parameter rather than using only precipitation data points. For different durations and different return periods, a precipitation process includes four precipitation time sequences. Each precipitation time sequence includes four precipitation data points (P_0, P_1, P_2, P_3), with each precipitation data point representing the precipitation of 1 day. The three data points, i.e., P_1, P_2, and P_3, represent the antecedent rainfall before the event, and P_0 represents the precipitation on that day. Then, the precipitation process is regarded as an input

Table 4 Value of peak GL for different return period storms when the duration of the rainfall is 6 h

Return period (year)	Peak GL before drainage tunnel completed	Peak GL after drainage tunnel completed	Cumulative rainfall (mm)
2	30.72	29.70	63
3	31.04	29.96	78
5	31.28	30.22	90
10	31.70	30.55	114
20	32.04	30.83	132
50	32.56	31.10	162
100	32.84	31.26	180

Table 5 Value of peak GL for different return period storms when the duration of the rainfall is 3 h

Return period (year)	Peak GL before drainage tunnel completed	Peak GL after drainage tunnel completed	Cumulative rainfall (mm)
2	30.43	29.49	51
3	30.65	29.68	63
5	30.97	29.90	75
10	31.29	30.17	90
20	31.60	30.41	105
50	31.99	30.71	123
100	32.24	30.87	138

Table 6 Value of peak GL for different return period storms when the duration of the rainfall is 1 h

Return period (year)	Peak GL before drainage tunnel completed	Peak GL after drainage tunnel completed	Cumulative rainfall (mm)
2	30.12	29.19	37
3	30.29	29.33	43
5	30.43	29.47	52
10	30.70	29.68	62
20	30.93	29.86	71
50	31.19	30.06	84
100	31.38	30.21	92

parameter for the PSO-SVM model. Four GL values could be obtained for one precipitation process, and each GL calculated represents the results of its corresponding 4 days of antecedent rainfall. The largest GL will be the peak groundwater level in the precipitation process. The values of peak GL for different return periods are shown in Tables 3, 4, 5, and 6.

The GL peaks of different return periods are presented in Tables 3, 4, 5, and 6. Then, the calculated GL peak is compared with critical GL (31 m) to estimate the motion state of the studied landslide. If the peak GL is larger than critical GL, the landslide will be considered to have a movement trend. If the calculated GL peak is smaller than critical GL, the landslide will be considered steady. By comparing the calculated peak GL and critical GL, the rainfall threshold of the studied landslide before and after the drainage tunnel was completed is also obtained. The rainfall thresholds before and after the drainage tunnel are shown in Fig. 13.

Before the drainage tunnel was completed, the rainfall threshold ranged from 63 to 78 mm, in contrast to the rainfall threshold, which ranged from 144 to 162 mm after the drainage tunnel was completed. The rainfall threshold after the drainage tunnel was completed is about twice the rainfall threshold before the drainage tunnel was completed. The rainfall threshold increased significantly because of the construction of the drainage tunnel. The rainfall thresholds are also compared with the IDF curves. The results of the comparison are shown in Fig. 14.

Figure 14 shows that both rainfall threshold curves are close to, or beyond, the lower value of return period curves when the duration is 24 h (e.g., 2-year return period and 10-year return period). Both rainfall threshold curves ascend toward higher values of the recurrence curves (100- to 10-year recurrences) when the duration is 1 h. These results are also in agreement with those presented in Huang (2013) and Wei et al. (2017, 2018). Huang (2013) investigated the rainfall thresholds for debris flow or landslides induced by Typhoon Morakot. The results also reveal that debris flows and landslides occur under a very wide range of rainfall characteristics, with return periods ranging from several years to 200 years.

The short-time and high intensity rainfall has been demonstrated as the necessary condition for triggering shallow landslides. For shallow landslides or debris flows, failure conditions can occur when, at a critical depth that is determined mainly by the apparent cohesion of the soil mass and the slope angle, the moisture content in the soil becomes close to saturation, resulting in a considerable reduction in the strength of the soil (Van Asch et al. 1999). Thus, the thresholds for triggering shallow landslides or debris flows usually are not sensitive to the total amount of rainfall; rather, they are controlled mainly by the intensity of the rainfall in a short period of time (Wei et al. 2017, 2018). For deep-seated landslides, the total amount of rainfall will be more important, as larger total

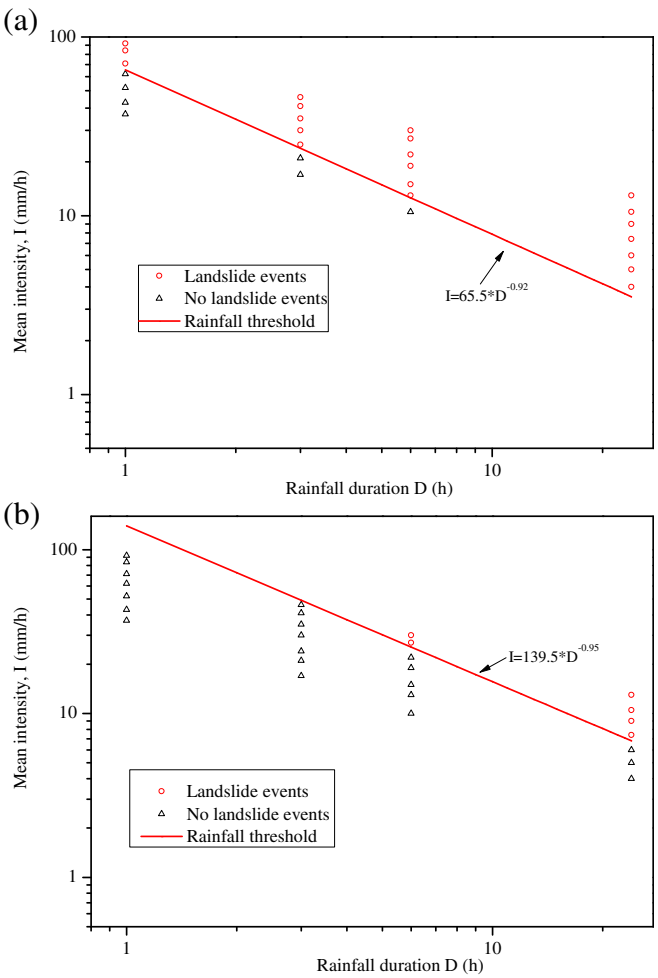

Fig. 13 Rainfall threshold of the studied landslide **a** before the drainage tunnel was completed and **b** after the drainage tunnel was completed

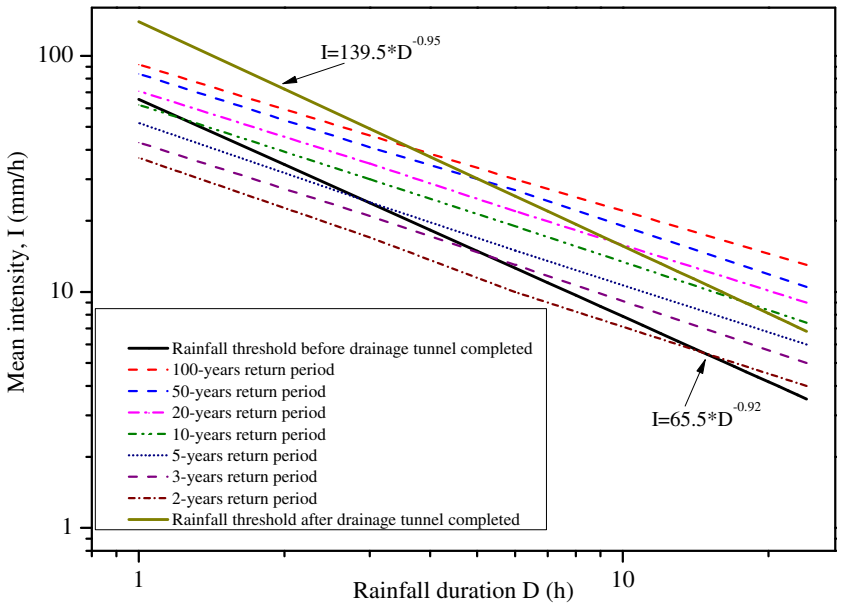

Fig. 14 Comparison between rainfall threshold and IDF curves

amount of rainfall usually resulting in larger increases in the groundwater level (Wei et al. 2019; Dai and Lee 2001).

However, for this deep-seated landslide case, due to the fact that the landslide body is broken rock mass (Sun et al. 2018), the conditions are favorable for the storage and infiltration of groundwater. Based on the monitoring data of the groundwater level and precipitation, Figure 7 shows that groundwater level is very sensitive to rainfall, and the speed of the hydrological response is very quick. The lag time between the time when the maximum precipitation occurred and the time when the groundwater level was at its highest level was small. A large precipitation event (duration may vary from 1 to 24 h) will induce a rapid increase in groundwater level. For the study of deep-seated landslides, the total amount of rainfall is more important than rainfall duration, as a larger total amount of rainfall usually results in larger increases in groundwater level. Accordingly, in this study, rainfall events with a large amount of rainfall (duration from 1 to 24 h) are considered for predicting the occurrence of deep-seated landslides.

Conclusion

This study examined data related to rainfall monitoring, groundwater level, and surface displacement and explored the effectiveness of a drainage tunnel in increasing the rainfall threshold of a deep-seated landslide. Firstly, the monitoring results show that the movement of the landslide under study was highly sensitive to the groundwater level (GL). The value of GL directly determines the motion state of the landslide. The value of critical GL that triggers rapid movement is 31 m. The monitoring data also show that the times to reach critical GL decreased significantly after the drainage tunnel was completed; in other words, the increase in GL was successfully controlled by the drainage tunnel. Then, the PSO-SVM model was developed to predict GL based on antecedent rainfall. The results show that the performance of the PSO-SVM model is acceptable. Based on the IDF curves, the rainfall thresholds of the landslide under study ranged from 63 to 78 mm before the drainage tunnel was constructed, in contrast to the rainfall threshold, which ranged from 144 to 162 mm after the drainage tunnel was completed. The rainfall threshold after the drainage tunnel was completed was about twice that of the rainfall threshold before the drainage tunnel was completed. The construction of the drainage tunnel significantly increased the rainfall threshold of the deep-seated landslide.

Funding information This research is financially supported by the National Natural Science Foundation of China (Grant No. 41772276), Key R&D project of Zhejiang Province (Grant No. 2017C03006), and China Postdoctoral Science Foundation (Grant No. 2019M652083).

References

Bogaard T, Greco R (2018) Invited perspectives: hydrological perspectives on precipitation intensity-duration thresholds for landslide initiation: proposing hydro-meteorological thresholds. Nat Hazards Earth Syst Sci 18(1):31–39

Bergh FVD, Engelbrecht AP (2006) A study of particle swarm optimization particle trajectories. Inf Sci 176(8):937–971

Conte E, Donato A, Pugliese L, Troncone A (2018) Analysis of the Maierato landslide (Calabria, Southern Italy). Landslides 15:1935–1950

Conte E, Troncone A (2018) A performance-based method for the design of drainage trenches used to stabilize slopes. Eng Geol 239:158–166

Cotecchia F, Lollino P, Petti R (2016) Efficacy of drainage trenches to stabilise deep slow landslides in clay slopes. Géotech Lett 6:1–6

Corominas J, Moya J, Ledesma A, Lloret A, Gili JA (2005) Prediction of ground displacements and velocities from groundwater level changes at the Vallcebre landslide (Eastern Pyrenees, Spain). Lanslides 2(2):83–96

Cortes C, Vapnik V (1995) Support-vector networks. Mach Learn 20(3):273–297

Dai FC, Lee CF (2001) Frequency–volume relation and prediction of rainfall-induced landslides. Eng Geol 59(3–4):253–266

Godt JW, Baum RL, Lu N (2009) Landsliding in partially saturated materials. Geophys Res Lett 36(2):206–218

Huang C (2013) Critical rainfall for typhoon-induced debris flows in the Western foothills, Taiwan. Geomorphology 185:87–95

Hong YM (2017) Feasibility of using artificial neural networks to forecast groundwater levels in real time. Landslides 3–4:1–12
Hong YM, Wan S (2011) Forecasting groundwater level fluctuations for rainfall-induced landslide. Nat Hazards 57(2):167–184
Iverson RM (2000) Landslide triggering by rain infiltration. Water Resour Res 36(7):1897–1910
Krkač M, Špoljarić D, Bernat S, Arbanas SM (2017) Method for prediction of landslide movements based on random forests. Landslides 14(3):947–960
Ji J, Zhang C, Gui Y, Lü Q, Kodikara J (2016) New observations on the application of LS-SVM in slope system reliability analysis. J Comput Civ Eng 31(2):06016002
Ledesma A, Corominas J, Gonzàles A, Ferrari A (2009) Modelling slow moving landslides controlled by rainfall. Proceeding of the 1st Italian workshop on landslides, Napoli. 1: 196–205
Li XZ, Kong JM (2014) Application of GA-SVM method with parameter optimization for landslide development prediction. Nat Hazards Earth Syst Sci 14(3):5295–5322
Lee LJE, Lawrence DSL, Price M (2006) Analysis of water-level response to rainfall and implications for recharge pathways in the chalk aquifer, SE England. J Hydrol 330(3):604–620
Mantovani F, Pasuto A, Silvano S, Zannoni A (2000) Collecting data to define future hazard scenarios of the Tessina landslide. Int J Appl Earth Obs Geoinf 2(1):33–40
Matti B, Tacher L, Commend S (2012) Modelling the efficiency of a drainage gallery workfor a large landslide with respect tohydrogeological heterogeneity. Can Geotech J 49:968–985
Park E, Parker JC (2008) A simple model for water table fluctuations in response to precipitation. J Hydrol 356(3–4):344–349
Rahardjo H, Hritzuk KJ, Leong EC, Rezaur RB (2003) Effectiveness of horizontal drains for slope stability. Eng Geol 69(3):295–308
Ren F, Wu X, Zhang K, Niu R (2015) Application of wavelet analysis and a particle swarm-optimized support vector machine to predict the displacement of the shuping landslide in the three gorges, China. Environ Earth Sci 73(8):4791–4804
Shackelford CD, Chang CK, Chiu TF (1994) The capillary barrier effect in unsaturated flow through soil barriers. Proceedings of the First International Congress on Environmental Geotechnics, Edmonton. pp:789–793
Sun HY, Wong LNY, Shang YQ, Shen YJ, Lü Q (2010) Evaluation of drainage tunnel effectiveness in landslide control. Landslides 7:445–454
Sun HY, Wu X, Wang DF, Xu HD, Liang X, Shang YQ (2018) Analysis of deformation mechanism of landslide in complex geological conditions. Bull Eng Geol Environ. https://doi.org/10.1007/s10064-018-1406-3
Van Asch, Buma J, Beek LPHV (1999) A view on some hydrological triggering systems in landslides. Geomorphology 30(1–2):25–32
Wang ZL, Shang YQ, Sun HY (2013) Optimal location and effect judgment on drainage tunnels for landslide prevention. J Cent South Univ 20:2041–2053
Wei ZL, Shang YQ, Zhao Y, Pan P, Jiang YJ (2017) Rainfall threshold for initiation of channelized debris flows in a small catchment based on in-site measurement. Eng Geol 217:23–34
Wei ZL, Xu YP, Sun HY, Xie W, Wu G (2018) Predicting the occurrence of channelized debris flow by an integrated cascading model: a case study of a small debris flow-prone catchment in Zhejiang province, China. Geomorphology 308:78–90
Wei ZL, Lü Q, Sun HY, Shang YQ (2019) Estimating the rainfall threshold of a deep-seated landslide by integrating models for predicting the groundwater level and stability analysis of the slope. Eng Geol 253:14–26
Zhang LL, Fredlund M, Fredlund DG, Lu HH, Wilson GW (2015) The influence of the unsaturated soil zone on 2-D and 3-D slope stability analyses. Eng Geol 193:374–383
Zhejiang Province Bureau of Hydrology (2003) Atlas of storms statistical parameters for Zhejiang Province. Hangzhou, Zhejiang. (in Chinese)
Zhi MM, Shang YQ, Zhao Y, Lü Q, Sun H (2016) Investigation and monitoring on a rainfall-induced deep-seated landslide. Arab J Geosci 9(3):182
Zhou C, Yin K, Cao Y, Ahmed B (2016) Application of time series analysis and PSO–SVM model in predicting the Bazimen landslide in the three gorges reservoir, China. Eng Geol 204:108–120

Z.-l. Wei · Y.-q. Shang · H.-d. Xu
College of Civil Engineering and Architecture,
Zhejiang University,
Hangzhou, 310058, China

H.-y. Sun (✉) · D.-f. Wang
Ocean College,
Zhejiang University,
Hangzhou, 310058, China
Email: shy@zju.edu.cn